Catalysis Today 145 (2009) 90–100

Contents lists available at ScienceDirect

Catalysis Today

journal homepage: www.elsevier.com/locate/cattod

Kinetic study of CO preferential oxidation over Pt–Rh/γ-Al_2O_3 catalyst in a micro-structured recycle reactor

Georgios Nikolaidis [a], Tobias Baier [a], Ralf Zapf [a], Gunther Kolb [a,*], Volker Hessel [a], Wilhelm F. Maier [b]

[a] Inistut für Mikrotechnik Mainz, Carl-Zeiss Strasse 18-20, 55129 Mainz, Germany
[b] Universität Saarbrücken, Lehrstuhl für Technische Chemie, 66123 Saarbrücken, Germany

ARTICLE INFO

Article history:
Available online 6 August 2008

Keywords:
Kinetic study
Preferential oxidation
CO
Microstructured
Recycle reactor

ABSTRACT

A micro-structured recycle reactor was developed for studying the kinetics of heterogeneously catalysed gas phase reactions. The preferential CO oxidation reaction over Pt–Rh/γ-Al_2O_3 catalyst in reformate surrogate containing up to 60 vol.% H_2 was investigated over a wide range of CO concentrations (0.5–2.0 vol.%) between one and four times O_2 excess (λ = 1–4). Initial concentration of H_2O and CO_2 were 2.5 vol.% and up to 20 vol.%, respectively, and their influence on the reaction rate was investigated as well. Measurements in a microreactor showed that the optimum temperature for the preferential oxidation process (PROX) was ~180 °C. Methanation and reverse water-gas shift reaction in this range were insignificant. The quantitative determination of CO oxidation rates as a function of CO, O_2, H_2 and CO_2 concentration between 150 °C and 190 °C led to reaction orders of −0.58 for CO and +0.88 for O_2, at an apparent activation energy of 92.9 kJ/mol. The addition of either H_2 or CO_2, decrease the CO oxidation rate.

The study of H_2 oxidation rate as a function of H_2, O_2 and CO revealed reaction orders of −0.26, 0.09 and −0.06, respectively.

1. Introduction

Microreaction technology is a relatively new concept which offers the possibility of miniaturization of conventional reactors while providing the same throughput. One of the first micro-structured devices was reported in literature in 1989. With the tools of micro-fabrication, several novel reactor configurations can be fabricated allowing different design concepts not feasible with conventional packed-bed technology. Such microchannel reactors or microreactors typically carry small channels with dimensions in the sub-millimeter range, which reduces diffusive transport limitations. This also results in a relatively large surface area-to-volume ratio and increased driving forces for heat and mass transport. This translates into short response times. The pressure drop in microchannels is substantially lower compared to packed-bed reactors. The unique flow and heat-/mass transfer properties have led to process improvements [1–10]. These benefits, however, need to be significant to counter-balance the higher production cost of microreactors compared to fixed-bed reactors.

Besides the application of microreactors as production devices, they bear advantages as laboratory tools for catalyst screening and for the determination of kinetics. The choice of a suitable reactor for carrying out experiments under conditions such that meaningful kinetic rate expressions can be obtained is of great importance. This is particularly true for catalytic reactions in which transport effects such as pore diffusion come into the picture, which make the scale-up of conventional fixed bed reactors from the laboratory to the pilot or even to the industrial scale a challenging task. This situation changes when micro-structured reactors are applied. Exactly the same optimum operating conditions as identified in the laboratory scale may be applied when scaling up the reactor. This is usually done by numbering up the channels in a much bigger reactor, which is consequently not "micro" anymore as far as outer dimensions are concerned. The channel dimensions and consequently the fluid-dynamic conditions within the channels remain the same.

For kinetic measurements, the integral reactor (plug flow reactor, PFR) is problematic, because it exhibits a concentration gradient and the solution of its material balance demands integration. On the other hand, the conversion of a differential reactor (continuous stirred tank reactor) represents directly the reaction rate and permits the derivation of simple algebraic reactor

* Corresponding author. Tel.: +49 6131 990 341.
E-mail address: kolb@imm-mainz.de (G. Kolb).

0920-5861/$ – see front matter © 2008 Elsevier B.V. All rights reserved.
doi:10.1016/j.cattod.2008.06.008

Nomenclature

AIC	Akaike's Information Criterion
$C(t)$	output concentration of gas (moles/l)
$C_1(t)$	inlet concentration of gas (moles/l)
Cat	catalyst
$[i]$	concentration of gas species i (vol.%)
E_A	activation energy (kJ/mole)
E	residence time distribution (s^{-1})
F_{in}	inlet flow rate (l/min)
F_R	recycle flow rate (l/min)
ΔH	reaction enthalpy (kJ/mole)
k_0	pre-exponential factor ($ml^{1-(\alpha+\beta+\gamma+\delta)}\, g_{cat}^{-1}\, s^{-1}$)
k_i	constants of species i (ml^{-1})
h_i	constants of species i (ml^{-1})
r	reaction rate ($ml\, g_{cat}^{-1}\, s^{-1}$)
R	universal gas constant ($kJ\, mole^{-1}\, K^{-1}$)
t_m	mean residence time (s)
T	temperature (K)
V	vessel volume (ml)
WHSV	weight hourly space velocity ($l\, h^{-1}\, g_{cat}^{-1}$)

Greek symbols

α	CO exponential factor in CO reaction rate
β	O_2 exponential factor in CO reaction rate
γ	H_2 exponential factor in CO reaction rate
δ	CO_2 exponential factor in CO reaction rate
θ_i	surface coverage of species i
κ	CO exponential factor in H_2 reaction rate
λ	O/CO ratio
ν	O_2 exponential factor in H_2 reaction rate
π	H_2 exponential factor in H_2 reaction rate
τ	residence time (s)

model equations. To approach the behaviour of an ideal continuously stirred tank reactor (CSTR), a recycle reactor must be constructed.

If a plug flow microreactor is operated in a way that most of the effluent stream is recycled, a small amount of feed is continuously added, and a small net-product stream continuously removed, a reactor system is obtained which has several advantages. By external or internal recycling of the gaseous phase, with recycle ratios (ratio of recycle flow and feed flow) greater than 25, perfect mixing can be achieved [11,12]. A further benefit lies in the fact that due to perfect mixing, that can be achieved at high recycle ratios, the material balances discharge like in the ideal, perfectly stirred CSTR. Perhaps the greatest advantage of this reactor type is its ability to control the catalysts temperature very accurately.

Theoretically, both the recycle reactors and CSTRs suit the above-described purposes equally well [2,12,13]. In practice the reactors used are never ideal; they can often be far from it. There are several reasons for this: the flow may have a preferential path in the tank, there may be dead zones in the tank, etc. [14]. The same applies to recycle reactors with internal circulation. External circulation may be achieved by mechanical recycle pumps as it is depicted in Fig. 1. Compared to internal circulation this setup has the advantage, that the recycle ratio is well-defined and easily determined.

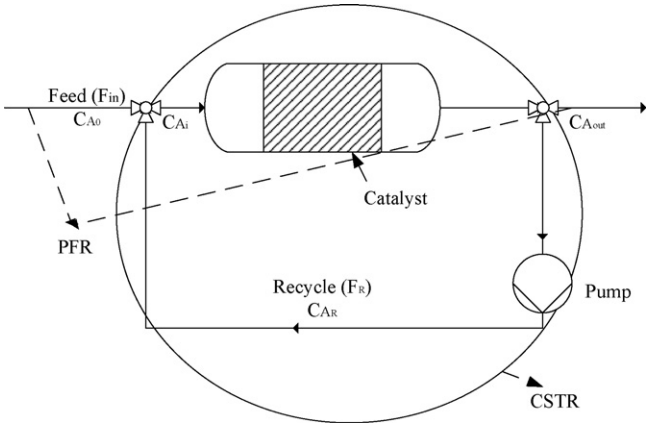

Fig. 1. Process diagram of a recycle reactor.

To make full use of the advantages and to avoid the difficulties associated with recycle reactors, one has to understand their performance characteristics and how this is related to the performance of commercial reactors. A basic requirement in the analysis of catalytic reactors is a rate expression for the reaction concerned. In the present paper we apply a recycle reactor for the study of the kinetics of the preferential oxidation of CO in the presence of O_2, H_2 and CO_2, i.e. for a gas composition equivalent to the reformate of a hydrocarbon reformer which was purified already by water-gas shift as first clean-up stage. A highly undesired side reaction in this case is the oxidation of hydrogen, which is also investigated.

The kinetic analysis was performed in three steps. Previously proposed reaction mechanisms were examined first, in order to derive the kinetic expressions. The second step comprises the setup of a suitable mathematical model and consists of two parts: firstly the selection of a reaction rate model and secondly the application of a suitable reactor model. Usually either power function models or hyperbolic models are used, the latter accounting for competitive adsorption of reactants.

The last step of the kinetic analysis consists in estimation of the model parameters. A comparison of results obtained from the parameter estimation method can be accomplished on the basis of the experimental test and of the quality of fits, which is affected by model errors, numerical errors and experimental errors.

2. Reactor and reaction system

2.1. Reactor characterization–residence time distribution

In order to predict the behavior of a reactor, the mass flow through the reactor should be determined. An ideally mixed reactor is by definition one that has identical concentrations at every point. A plug flow shows no mixing in the direction of the flow. Practical systems are often modeled by combining ideally mixed and plug flow reactors.

The residence time distribution (RTD, also exit age distribution), $E(t)$, indicates the time the fluid elements of a stream remain in the reactor and has the units of $time^{-1}$. It is convenient to represent the RTD as normalized distribution as shown in Fig. 2.

For comparison purposes, the mean residence time (t_m) was calculated by integrating the RTD:

$$t_m = \int_0^\infty t\, E(t)\, dt \quad (1)$$

The recycle loop has a defined volume V (cm^3) through which the fluid flow F_R (cm^3/s) is passed. The tracer introduced into the fluid

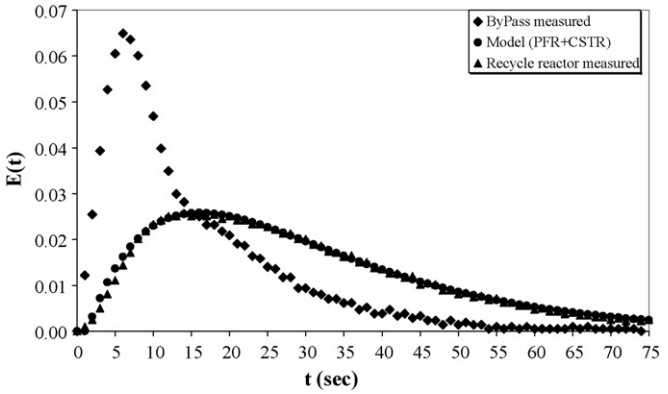

Fig. 2. Residence time distribution for a plug flow reactor followed by a continuous stirred tank reactor.

entering the reactor, and the concentration of tracer leaving the reactor is recorded. The material balance of a CSTR is defined as follows:

$$V\frac{dC(t)}{dt} = F_R(C_1(t) - C(t)) \tag{2}$$

where C and C_1 are, respectively, the output and the inlet concentration of the gas in moles/l.

Dividing both sides with F_R and applying Laplace transformation the equation becomes:

$$G(s) = \frac{1}{(V/F_R)s + 1} = \frac{1}{\tau s + 1} \tag{3}$$

where V/F_R is the residence time τ. The inverse transform gives the time-domain response (residence time distribution):

$$g_{CSTR}(t) = \frac{1}{\tau_{CSTR}} e^{-(t/\tau_{CSTR})} \tag{4}$$

Applying the same for a plug flow reactor we get:

$$g_{PFR}(t) = t - \tau_{PFR} \tag{5}$$

For a system consisting of a series operation of a PFR and CSTR the overall transform equation derives by multiplying the individual transfer functions in their Laplace transformed form and applying the inverse Laplace transformation on the result [15].

Experimentally, the residence time distribution can be determined easily and directly by a widely used method of inquiry, the stimulus–response experiment [14]. Such marker experiments provide the age distribution of the molecules in a flow. The marker must fulfill certain requirements: it must not affect the bulk flow of the process, it must mix perfectly with the bulk flow and one must be able to measure it. To find the E curve for a recycle reactor pulse experiments were performed. The results of these experiments will be discussed in Section 4.1.

2.2. Reaction system

During the selective oxidation of CO in the presence of H_2, water is formed as an undesired by-product:

Desired reaction:

$$CO + \tfrac{1}{2}O_2 \rightarrow CO_2 \quad (\Delta H_{298\,K} = -283\,kJ/mole) \tag{6}$$

Undesired reaction:

$$H_2 + \tfrac{1}{2}O_2 \rightarrow H_2O \quad (\Delta H_{298\,K} = -242\,kJ/mole) \tag{7}$$

For later reference we define the λ ratio as the ratio between atomic oxygen and carbon monoxide concentrations in the inlet stream:

$$\lambda = \frac{2[O_2]}{[CO]} \tag{8}$$

The overall reaction in the CO oxidation process includes Eqs. (9)–(11). On precious metal surfaces (e.g. Pt and Rh) the CO oxidation reaction is generally believed to follow a mechanism of the following type:

$$CO_{(g)} \leftrightarrow CO_{(ads)} \tag{9}$$

$$O_{2(g)} \leftrightarrow 2O_{(ads)} \tag{10}$$

$$CO_{(ads)} + O_{(ads)} \xrightarrow{(rds)} CO_{2(ads)} \xrightarrow{fast} CO_{2(g)} \tag{11}$$

CO desorption from these surfaces is relatively fast so the surface reaction between the two adsorbed species becomes rate determining step (rds) [16].

If the two adsorbed molecules are mobile on the surface and intermix freely, the rate of the reaction will be determined by the following rate expression for the bimolecular surface combinations step:

$$r_{CO} = k\,\theta_{CO}\,\theta_O, \tag{12}$$

where θ_i are the surface concentrations of the two species absorbed on their respective reaction sites.

In case where CO adsorbed as molecule and O_2 adsorbed dissociatively, are competing for the same adsorption sites then the relevant rate expression is [17]:

$$r_{CO} = \frac{k_0\, e^{-(E_A/R)((1/T)-(1/T_{mean}))}\,[CO]^{\alpha}\,[O_2]^{\beta}}{(1 + k_1[CO] + k_2[O_2]^{0.5})^2} \tag{13}$$

where T_{mean} is the average value of the temperatures measured during each set of experiments.

In the model considered and described by Eq. (13), molecules were assumed to compete for sites of one kind. In case where molecules adsorb independently on sites of different kinds; e.g., two site types, one for CO the other for O_2 rate expression (12) becomes:

$$r_{CO} = \frac{k_0\, e^{-(E_A/R)((1/T)-(1/T_{mean}))}[CO]^{\alpha}[O_2]^{\beta}}{(1 + k_1[CO] + k_2[O_2]^{0.5})(1 + k_3[CO] + k_4[O_2]^{0.5})} \tag{14}$$

In reality one species is only adsorbed at one type of sites, but we leave here the more general expression. Both models leave only the partial pressure of CO and O_2 in the reaction term. However, as mentioned before, the CO oxidation reaction is frequently applied for the purification of reformer off-gas dedicated for PEM fuel cell supply owing to the very limited CO tolerance of low temperature PEM fuel cell catalysts [2]. In case steam reforming is applied, the reformate contains not only CO but also H_2, CO_2 and steam [18]. Therefore not only the kinetics of CO oxidation was under investigation in the current paper but also the effect of these reactants. Thus, we may assume the rate of the CO oxidation as

$$r_{CO} = \frac{k_0\, e^{-(E_A/R)((1/T)-(1/T_{mean}))}[CO]^{\alpha}[O_2]^{\beta}[H_2]^{\gamma}[CO_2]^{\delta}}{(1 + k_1[CO] + k_2[O_2]^{0.5} + k_5[H_2]^{0.5} + k_6[CO_2])^2} \tag{15}$$

for one common site or similarly for two site types:

$$r_{CO} = \frac{k_0\, e^{-(E_A/R)((1/T)-(1/T_{mean}))}[CO]^{\alpha}[O_2]^{\beta}[H_2]^{\gamma}[CO_2]^{\delta}}{(1 + k_1[CO] + k_2[O_2]^{0.5} + k_5[H_2]^{0.5} + k_6[CO_2])\,(1 + k_3[CO] + k_4[O_2]^{0.5} + k_7[H_2]^{0.5} + k_8[CO_2])} \tag{16}$$

There are effects that are hard to be included in an analytical model. Namely, although CO_{ad} and O_{ad} are not adsorbed on the same sites, they affect each other since the two sites are too close to each other. Additionally CO_{ad} coverage on Pt depends on the surface orientation and the interactions of the adsorbates are not taken into consideration. Thus, inherent simplifications were necessary in the model.

The addition of H_2 and CO_2 strongly affects the k_0 parameter. The question still remains, how H_2 and CO_2 are participating in the reaction rate equation and whether it is possible to construct a model that could describe the oxidation of CO independently of the presence of CO_2 and/or H_2. By means of nonlinear regression for all the experimental data obtained we can construct an overall model that could represent all the three cases, within the reaction parameter range tested, equally well.

When fitting experimental data with regression, the main objective is to discriminate between different models or to test whether the data are more consistent with one possible mechanism relative to another. A statistic method for comparing models is Akaike's Information Criterion, abbreviated AIC [19]. Accepting the assumption of regression, the AIC is defined by the following equation:

$$\mathrm{AIC} = N \ln\left(\frac{\mathrm{SS}}{N}\right) + 2K \tag{17}$$

where N is the number of data points, K is the number of parameters fit by the regression plus one and SS is the sum of the squares of the residuals of the regression. The model with the lower AIC score is the model more likely to be correct [19]. If the AIC scores are very close, there is not much evidence to choose one model over the other. The probability to choose the correct model is computed by the following equation, where Δ is the difference between AIC scores [19]:

$$\text{probability} = \frac{e^{-0.5\Delta}}{1 + e^{-0.5\Delta}} \tag{18}$$

3. Experimental

The setup applied for the kinetic studies consisted of a number of thermal mass flow controllers (BRONKHORST), which ensured a steady flow of gases needed. The feed gases were mixed in the tubing upstream before the reactor by turbulent flow.

Tests were carried out at 1.3 bar of pressure. For experiments carried out without H_2 and CO_2 in the reaction mixture, the feed consisted of 0.5–2.0 vol.% CO, O_2 (depending on λ), and N_2 in balance. For experiments carried out with H_2 in the reaction mixture, the feed was composed by 0–60 vol.% H_2, 0.5–2.0 vol.% CO, O_2 (depending on λ ratio), and N_2 in balance. Finally, the feed simulating the reformate stream in presence of CO_2 consisted of 0–60 vol.% H_2, 0–20 vol.% CO_2, 0.5–2.0 vol.% CO, O_2 (depending on λ ratio), and N_2 in balance. The ratio of N_2 to O_2 in the feed was approximately that of air as it would be the case in a fuel processor. It was only varied when carrying out experiments with different λ and it was kept below 4. These differences, though, are not considered to have any influence on the results. All feed components were preheated before entering the micro-structured device.

When steam was added to the feed, bi-distillated water was fed from tanks to a micro-structured electrically heated laboratory evaporator at 150 °C. The evaporator was fed by a thermal mass flow meter. It carried channels of very low dimensions (about 30 μm) to achieve stable evaporation of the small flow rates applied. To avoid condensation and minimize adsorption at the steel surface, all tubing and valves were heated to temperatures exceeding 120 °C.

The test reactors applied have a sandwich design with two micro-structured platelets being attached face to face. The platelets carried 14 channels each, which were 25 mm long, 500 μm wide and 250 μm deep. The channels together with the inlet and outlet region were prepared by wet chemical etching. Each couple of platelets was coated with the catalyst and subsequently sealed by laser welding. A more precise description of the reactor was published elsewhere [7]. The reactor was externally heated by heating cartridges. Owing to the big mass of the heaters, isothermal conditions could be achieved. The Pt–Rh/Al_2O_3 catalyst [20] was prepared according to the procedure described in [21]. The total mass of Pt–Rh/Al_2O_3 catalyst, developed by IMM was 8.97 mg. The same catalyst sample had passed a 1000-h stability test prior to the experiments [2] described here and thus a stable performance was expected. In addition, to ensure that during the experiments no catalyst-deactivation occurred, activity-tests of the catalyst were performed after each set of experiments by simply isolating the reactor from the recycle-loop using two valves installed, as depicted in Fig. 1.

To generate the recycle flow a hermetic metal-bellows pump was used (Metal Bellows, Senior Operations, Inc., MB-HT 21 H.T. P/N 40075/27508). The pump was temperature-resistant up to 220 °C and suitable for dosing explosive mixtures (here hydrogen and oxygen). The pump was heated by a heating cable to a temperature similar to that of the reactor.

The pump could achieve recycle flow rates up to 4 l/min at a net feed flow rate of 100 ml/min. This corresponded to a recycle ratio of 40 (40 × 100 ml/min = 4000 ml/min). A recycle ratio near 35 was chosen which was regarded sufficient to simulate an ideal CSTR [13].

The extent of reaction per pass through the catalyst was very small; consequently isothermal conditions could be maintained throughout the reactor. The high recycle rates applied excluded mass transfer limitations.

High recirculation rates also permit high gas velocities over the catalyst coating without the use of excessive quantities of reactants. Thus, mass transfer limitations can be eliminated even for very rapid reactions. Assuming that the overall rate of reaction is limited at low recirculation ratios by the rate of mass transfer, when a certain recirculation ratio is exceeded the total conversion remains constant and a change of recirculation ratio has no effect on the conversion (Fig. 3). Since the CO conversion was independent from the flow rate and thus from the recirculation rate, mass transfer limitation were not to be expected.

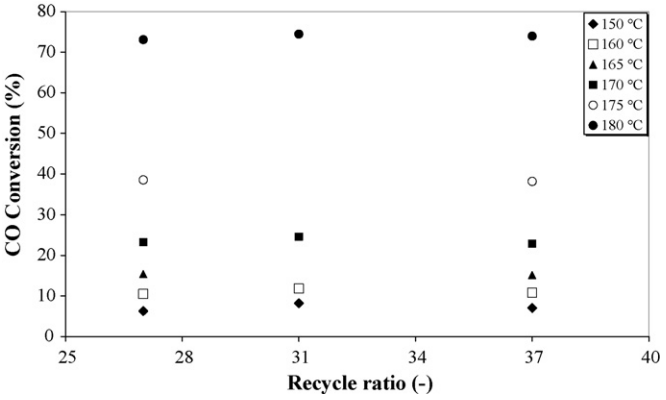

Fig. 3. Effect of recirculation rate on CO conversion (0.5% CO, $\lambda = 4$ and N_2 in balance).

The flow rate of 3.5 l/min in the recycle loop was very high and corresponded to a WHSV of =24080 l/(h $g_{catalyst}$). To achieve stable and full conversion of CO, the catalyst applied had to be operated at a WHSV ~200 l/(h $g_{catalyst}$) in fuel processing applications. Thus, by applying a recycle ratio of 35, the conversion achieved did not exceeded 15%.

To ensure that a specific quantity of tracer was entering the reactor a valve actuator (GILSON Valvemate Rheodyne 7010) was applied for the determination of the RTD.

It consisted of a conventional six-port sample valve, which was used to inject the tracer into the continuous flow passing through the reactor. An excess of tracer was applied to load the sample loop of the sample injector to ensure that the sample loop was completely filled with tracer.

The tracer-quantity (sample loop volume) used in RTD experiments amounted to 9 μl.

For the RTD measurements CO_2 was selected as suitable inert chemical tracer. A reactor uncoated with catalyst was used to avoid adsorption of CO_2 inside the catalyst's pores. For measuring the tracer concentration, a CO_2 IR-Sensor (Winter GmbH Gas-Warnanlagen, Transducer TCOD-IR-5, Item No. 85785) connected with a data logger (Testo 125) for online measurement was used. Standard measuring range of the sensor was 0–5 vol.% and the dead volume of the device was 0.5 ml. Response time was below 1 s and the signal output between 4 mA and 20 mA in logarithmic scale.

For the determination of the reaction rates, the product composition was monitored by online gas chromatography (Varian CP-4900 Micro-GC). It consisted of four different channels each with a separate TCD detector and oven. Channel 1 had a 10-m-long Molsieve column which could separate O_2, N_2 and CO, channel 2 had a similar column to separate H_2 and CH_4, channel 3 had a Porapak U column to separate CO_2, H_2O and HC-species up to butane. Channel 4 was not used. All channels used helium as carrier gas with the exception of channel 2 which used N_2 as carrier gas. The column pressure was in all cases 150 kPa. Each analysis lasted for 1 min while it was possible to have an analysis cycle of ca. 1.5 min.

4. Results

4.1. Determination of the residence time distribution

Fig. 2 shows the results from the RTD measurements performed at a feed flow rate of 100 ml/min through the recycle reactor at recycle ratio of 35. The tracer signal fed to the reactor was determined in bypass and fed to the reactor. A certain delay of the reactor response was observed (see Fig. 2) which was thought to originate from the tube upstream the recycle reactor loop, which connected the sample loop with the recycle reactor. This tube was modeled as PFR (see Fig. 1). The results obtained with this model (PFR + CSTR) revealed best agreement between predicted and experimentally determined reactor response. Table 1 provides a comparison of model parameters (reactor volumes) and the actual values of the experimental setup.

The good agreement of the model with the experiments justifies the assumption that the recycle loop behaves as an ideally mixed CSTR. However the actual reaction takes place only in the microreactor.

4.2. Kinetic model development for CO oxidation reaction

In the following, the conversion of the CO oxidation in simulated reformer gas and the effect of other species on reaction rate are discussed. The standard method for the determination of reaction orders is to vary the partial pressure or concentration of one of the reactants, while keeping all other reactants constant. In the present study, however, this approach was not always followed, since it would entail measurements over a large range of λ-values, which is undesirable for two reasons: (a) prime criterion for the preferential CO oxidation is the minimization of H_2 oxidation so that the relevant range of λ-values is limited (λ ~ 1–4) and (b) a large variation implies different reaction regimes, which would invalidate the experimental approach because of a change in mechanism [19,22–25]. Nevertheless one can determine reaction rates in the range λ = 1–4.

Table 1
Characteristics of the PFR + CSTR model applied

	PFR	CSTR	
	Pipe	Real	Model
Volume (ml)	1.6	17.4	17.6
Residence time (s)	1.3	14.4	14.6
Sum of squared errors/number of data points	10^{-7}		

The effect of the other reactants usually present in PROX, namely H_2, CO_2 and H_2O on the reaction rate of CO oxidation were determined. For all experiments performed the reactor exhaust consisted only of H_2, CO_2, CO, H_2O, O_2 and N_2.

4.2.1. CO oxidation without H_2

The data for estimation of the parameters were obtained with the catalyst containing 5 wt.% Pt and 5 wt.% Rh over γ-Al_2O_3. Conversion at the maximum temperature was 15% as it can be seen from Fig. 4. The ranges of the experimental conditions covered are listed in Table 2.

Several model cases were evaluated. Table 3 shows the parameters estimated for each one referring to the basic kinetic equation (17), see Section 2. The model with the lowest AIC score was then chosen to describe the CO oxidation. It turned out that Eq. (17) without any adsorption terms was sufficient to describe the measurements:

$$r_{CO} = k_0\, e^{-(E_A/R)((1/T)-(1/T_{mean}))}[CO]^{\alpha}[O_2]^{\beta} \quad (19)$$

All parameters required can be readily determined by nonlinear regression. The reaction order with respect to CO concentration based on Eq. (13) was $\alpha = -0.53$. This is in reasonable agreement with the data found in literature [19,22,23]. Fig. 4 shows the temperature dependence of the conversion in the range of 150–180 °C. The apparent activation energy from the nonlinear

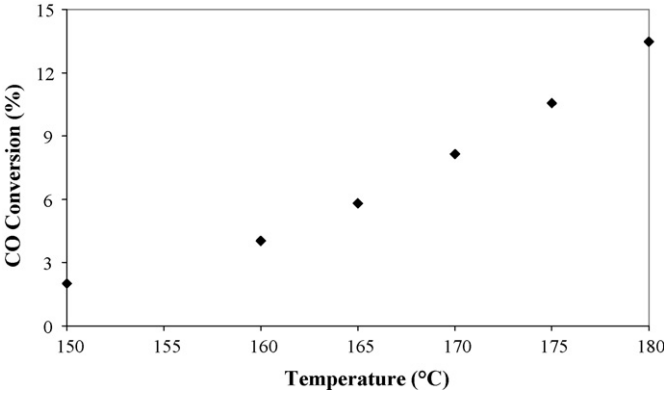

Fig. 4. CO conversion over Pt–Rh/γ-Al_2O_3 catalyst (1.5 vol.% CO, λ = 3 and N_2 in balance).

Table 2
Range of experimental conditions during the CO oxidation over Pt–Rh/γ-Al_2O_3

Total feed (ml/min)	100
CO (ml/min)	0.5–2.0
λ ratio	1.0–4.0
T (°C)	150–180

N_2 in balance.

Table 3
Models tested for the CO oxidation over Pt–Rh/γ-Al_2O_3 (31 data points)

Model no.	k_1	k_2	k_3	k_4	AIC
1.	–	–	–	–	20.24
2.	–	+	–	–	22.20
3.	–	+	+	–	24.90
4.	+	+	–	–	22.24
5.	+	–	–	–	23.55
6.	+	+	+	–	27.81
7.	+	+		+	29.32
8.	+	+	+	+	31.34

Table 4
Confidence intervals of the kinetic parameters estimated for CO oxidation without H_2

	Model no. 1
α	-0.53 ± 0.13
β	0.79 ± 0.05
E_A (kJ/mol)	94.2 ± 6.5
T_{mean} (K)	436.7
k_0 ($ml^{0.74}\, g_{cat}^{-1}\, s^{-1}$)	34.5 ± 17.6

regression was 94.2 kJ/mole (see also Fig.5a). The parameters of Eq. (14) are summarized in Table 4. The confidence interval is 95%.

From these calculated parameters, the rate-model becomes:

$$r_{CO} = 34.49\, e^{-(94.2/R)((1/T)-(1/436.7))}[CO]^{-0.53}[O_2]^{0.79}\ ml\, CO\, g_{cat}^{-1}\, s^{-1} \quad (20)$$

Fig. 5b shows a parity plot of the measured values and the data gained with the model described by Eq. (20).

The experiments described above revealed that the velocity of the CO oxidation reaction in the presence of CO, O_2 and N_2 was proportional to the concentration of O_2, but inversely proportional to the pressure of CO. This indicates reaction inhibition through CO, most likely due to competitive adsorption. Such a reaction behavior has been described before [22–26]. The model is limited to the present parameter range presented in Table 2.

4.2.2. CO oxidation in the presence of H_2

The data for estimation of the parameters for CO oxidation in the presence of H_2 were obtained over the same catalyst sample (5 wt.% of Pt and 5 wt.% of Rh over γ-Al_2O_3). The range of experimental conditions covered is listed in Table 5.

As it is shown in Fig. 6, for the oxidation of CO the conversion in the presence of H_2 was lower than without H_2. Two possible reasons for this behavior are competitive adsorption and reaction or removal of reactive O_2 by H_2.

The system of molecularly adsorbed CO and atomically adsorbed H_2, co-adsorbed on metal surfaces provides mutual interactions [27]. The difference in adsorption strength between CO and H_2 provides a situation where CO dominates the noble metal surface when both gases are present. The H_2 competition with CO for a noble metal site is much less favorable due to its lower adsorption strength, but its high concentration (here 60 vol.%) relative to CO (<2 vol.%) in the reformate may result in

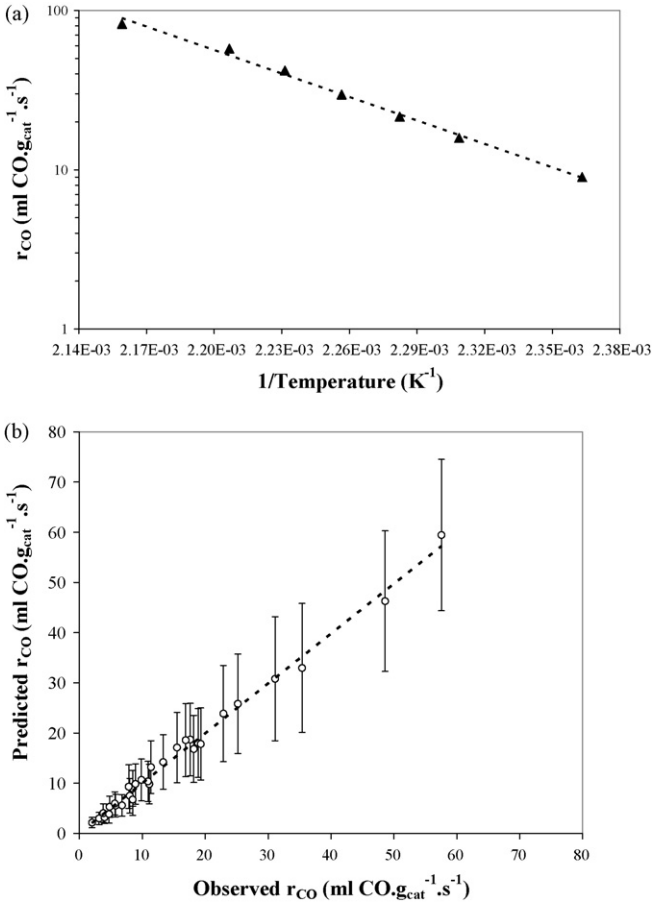

Fig. 5. (a) Arrhenius plot for CO oxidation in the presence of CO, O_2 and N_2 (λ = 4, 2.0 vol.% CO and N_2 in balance) and (b) parity plot for the CO oxidation in presence of O_2, CO and N_2 in balance.

Table 5
Range of experimental conditions during the CO oxidation in the presence of H_2

Total feed (ml/min)	100
CO (ml/min)	0.5–2.0
λ ratio	1.0–4.0
H_2 (ml/min)	0–60
T (°C)	150–180

N_2 in balance.

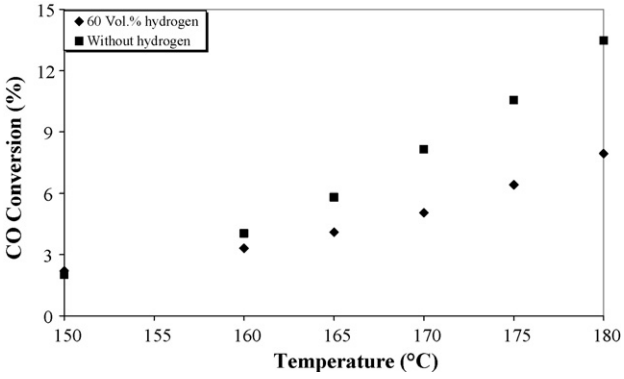

Fig. 6. CO conversion over Pt–Rh/γ-Al_2O_3 catalyst (60 vol.% H_2, 1.5 vol.% CO, λ = 3 and N_2 in balance).

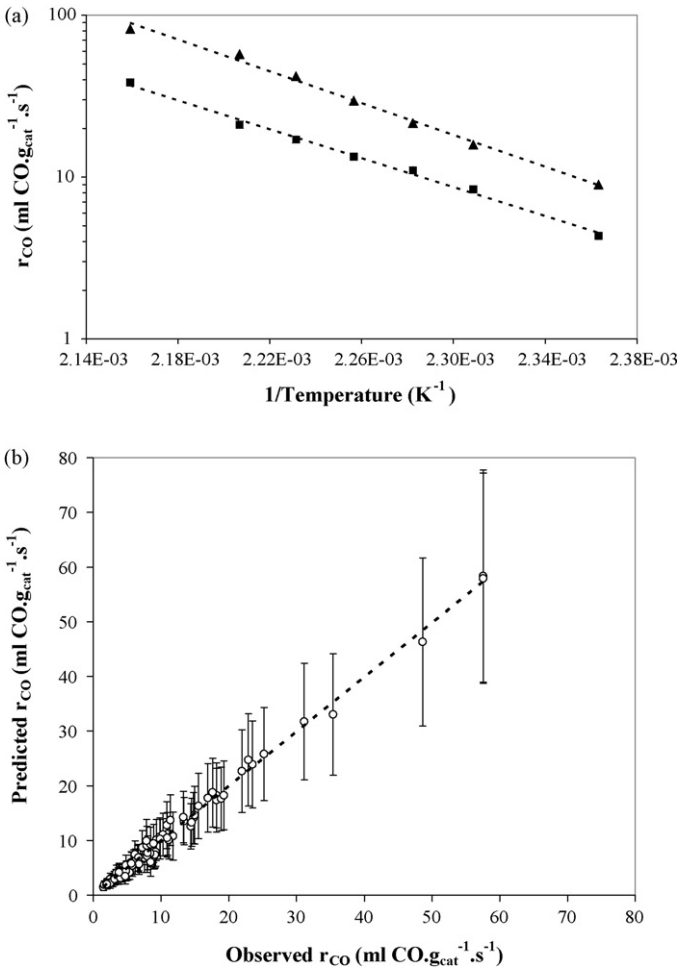

Fig. 7. (a) Arrhenius plot for CO oxidation and the influence of H_2 on the reaction rate constant (λ = 4, 2.0 vol.% CO and N_2 in balance): (▲) without H_2 and (■) with 60 vol.% H_2 and (b) parity plot for the CO oxidation in presence of CO, O_2, H_2 and N_2 in balance.

a reduced surface coverage of CO [28]. Even though H_2 was oxidized in the reactor, the H_2 conversion was low and the H_2 concentration throughout the reactor did not vary significantly, as is typical under preferential CO oxidation conditions. It is reported that the effect of H_2 on the CO oxidation rate depends on the support material and on the metal surface as well [22,29].

Fig. 7a shows the temperature dependence of the rate in the range of 150–180 °C. The model cases examined are presented in Table 6. The calculations also included data points of the CO oxidation in absence of hydrogen.

The model with the lowest AIC score was then chosen to describe the CO oxidation. Thus, the oxidation of CO in the presence of H_2 is described by the following equation:

$$r_{CO} = \frac{k_0\, e^{-(E_A/R)((1/T)-(1/T_{mean}))}[CO]^{\alpha}[O_2]^{\beta}}{1 + k_2[O_2] + k_5[H_2]^{0.5}} \quad (21)$$

Table 7 shows the kinetic parameters along with their 95% confidence interval for the model that best fit the experimental data.

The 2nd model had the lower AIC score and there was 66% probability that it was the more likely to be correct. However, the model is limited to the present parameter range presented in Table 5. Hence, the reaction rate of CO oxidation in the presence or in the absence of H_2 can be generalized and described by the following equation:

$$r_{CO} = \frac{64.3\, e^{-(93.2/R)((1/T)-(1/438.06))}[CO]^{-0.63}[O_2]^{0.98}}{1 + 10.6[O_2] + 2.1[H_2]^{0.5}}\ \text{ml CO}\, g_{cat}^{-1}\, s^{-1} \quad (22)$$

A parity plot comparing the measured values with the model described by Eq. (22) is shown in Fig. 7b for the whole temperature range under investigation.

The mechanism proposed, suggests reaction between CO adsorbed on one site (e.g. Pt) and O_2 on the other. In Eq. (22) the O_2 adsorption rate was taken to be proportional to θ_O (rather than the expected θ_O^2 dependence) in view of the observation of Yates et al. [30] that the θ_O dependence describes more precisely the rate of O_2 adsorption on Rh. This choice of first-order O_2 adsorption kinetics was also supported by our kinetic data; as second-order O_2 adsorption kinetics could not match the CO oxidation rate equally well (higher AIC).

Table 6
Models tested for the CO oxidation in the presence of H_2 over Pt–Rh/γ-Al_2O_3 (82 data points)

Model no.	k_1	k_2	k_3	k_5	k_7	AIC
1.	+	+	–	+	–	14.98
2.	–	+	–	+	–	9.16
3.	–	–	–	+	–	19.16
4.	–	+	–	–	–	12.44
5.	+	+	–	–	+	15.73
6.	–	+	–	–	+	11.58
7.	–	+	+	+	–	15.58
8.	–	+	+	–	+	16.64

Table 7
Confidence intervals of the kinetic parameters estimated for CO oxidation in the presence of H_2

	Model no. 2
α	-0.63 ± 0.08
β	0.98 ± 0.1
E_A (kJ/mol)	93.2 ± 3.5
T_{mean} (K)	438.06
k_0 ($ml^{0.65}\, g_{cat}^{-1}\, s^{-1}$)	64.3 ± 26.4
k_2 (ml^{-1})	10.6 ± 4.2
k_5 (ml^{-1})	2.1 ± 0.4

4.2.3. CO oxidation in the presence of H_2 and CO_2

In order to determine the kinetics of preferential oxidation of CO in realistic reformate, experiments were performed in the presence of CO_2.

The range of experimental conditions covered is listed in Table 8.

The inhibition effect of CO_2 on the preferential oxidation of CO was strong. The presence of CO_2 influenced in negative way the oxidation and hence participated in the reaction rate equation in the denominator. Fig. 8a shows the temperature dependence of the rate in the range of 150–180 °C. The model cases examined are presented in Table 9 referring to Eq. (19). They also include all data points of the former model (see Section 4.2.2).

Nonlinear regression analysis of the models presented in Table 9, described by Eq. (16), shows that γ, δ, k_1, k_3, k_4, k_7 and k_8 parameters were statistically not significant. They were therefore

Table 8
Range of experimental conditions during the CO oxidation in the presence of H_2 and CO_2

Total feed (ml/min)	100
CO (ml/min)	0.5–2.0
λ ratio	1.0–4.0
H_2 (ml/min)	0–60
CO_2 (ml/min)	0–20
T (°C)	150–190

N_2 in balance.

removed from the model and the data were fitted once again. The influence of both H_2 and CO_2 were found to be negative as expected.

AIC scores of the models indicated that there was 98% probability that model no. 4 was more likely to be correct and thus was chosen to describe the CO oxidation in the presence of H_2 and CO_2. The model is described by the following equation:

$$r_{CO} = \frac{k_0\, e^{-(E_A/R)((1/T)-(1/T_{mean}))}[CO]^{\alpha}[O_2]^{\beta}}{1 + k_2[O_2] + k_5[H_2]^{0.5} + k_6[CO_2]} \quad (23)$$

The parameters obtained in nonlinear regression together with their 95% confidence intervals are summarized in Table 10.

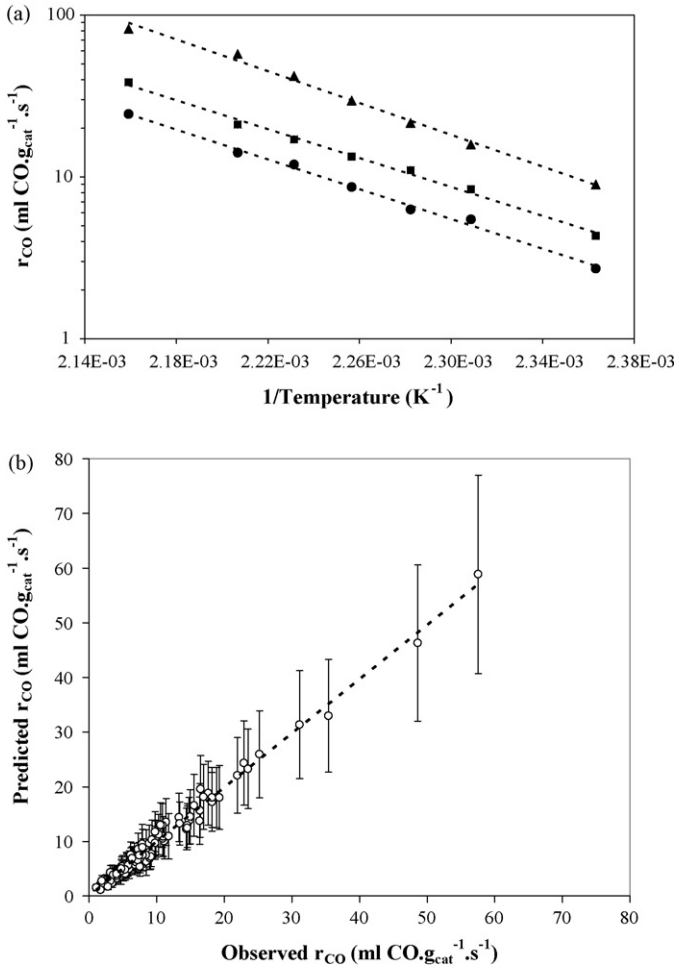

Fig. 8. (a) Arrhenius plot for CO oxidation and the influence of, H_2 and CO_2 on the reaction rate constant (λ = 4, 2.0 vol.% CO and N_2 in balance): (▲) without H_2 and CO_2, (■) with 60 vol.% H_2 and (●) with 60 vol.% H_2 and 15 vol.% CO_2 and (b) parity plot for the CO oxidation in the presence of CO, O_2, H_2, CO_2 and N_2 in balance.

Table 9
Models tested for the CO oxidation in the presence of H_2 and CO_2 over Pt–Rh/γ-Al_2O_3 (116 data points)

Model no.	k_2	k_5	k_6	k_7	k_8	AIC
1.	–	+	+	+	+	178.44
2.	–	+	+	–	–	27.75
3.	–	+	–	–	+	36.15
4.	+	+	+	–	–	26.51
5.	+	+	+	+	+	34.53
6.	+	+			+	29.62

Table 10
Confidence intervals of the kinetic parameters estimated for CO oxidation in the presence of H_2 and CO_2

	Model no. 4
α	-0.58 ± 0.08
β	0.88 ± 0.09
E_A (kJ/mol)	92.9 ± 3.5
T_{mean} (K)	441.2
k_0 ($ml^{0.7}\, g_{cat}^{-1}\, s^{-1}$)	60.0 ± 21.5
k_2 (ml^{-1})	4.4 ± 2.9
k_5 (ml^{-1})	1.9 ± 0.3
k_6 (ml^{-1})	20.5 ± 3.8

Thus, the rate equation takes the following form:

$$r_{CO} = \frac{60\, e^{-(92.9/R)((1/T)-(1/441.18))}[CO]^{-0.58}[O_2]^{0.88}}{1 + 4.4[O_2] + 1.9[H_2]^{0.5} + 20.5[CO_2]}\ ml\ CO\ g_{cat}^{-1}\ s^{-1} \quad (24)$$

The partial reaction order of CO was determined to be slightly lower than the order determined without CO_2, approximately −0.58 instead of −0.63. Nevertheless, the error of two results (with and without CO_2 in the feed) overlap with each other, -0.58 ± 0.04 (with CO_2 in the feed) and -0.63 ± 0.05 (without CO_2 in the feed), hence, are statistically tied. The same applies to the apparent activation energy values; i.e. within errors, the activation energies are not widely different. From nonlinear regression analysis, we can extract the activation energy of 92.9 kJ/mol, which is similar to the values found in previous cases.

The decrease of the reaction rate in the presence of CO_2 is in agreement with literature [19] and can also be explained by the existence of the large amounts of CO_2 being present on the catalyst's surface (similar to H_2 effect), which partially blocks the adsorption of all remaining reactants (here CO, O_2 and H_2) [31–33]. The same can occur if large amounts of O_2 would be present. As long as O_2 exists in reasonable concentrations (i.e. λ below 4) its contribution in the denominator is small and the CO reaction rate is not strongly affected by this factor.

The above model can be applied also in cases where no H_2 or CO_2 is present in the reaction mixture by simply setting their values to 0 ($[H_2] = 0$ and/or $[CO_2] = 0$). A comparison between observed and predicted values, by the model described here, of CO oxidation rate is shown in a parity plot (Fig. 8b).

4.2.4. CO oxidation in the presence of H_2, CO_2 and steam

To examine the influence of steam on the reaction, experiments were performed at temperatures exceeding 120 °C to avoid any condensation. As shown in Fig. 9, H_2O had a dramatic effect on CO conversion between the temperatures of 120 °C and 160 °C. At a temperature of 130 °C, no reaction was observed at all and thus, conversion was 0% when no steam was present in the feed while it reached 2% when 2.5 vol.% water was added. In the temperature

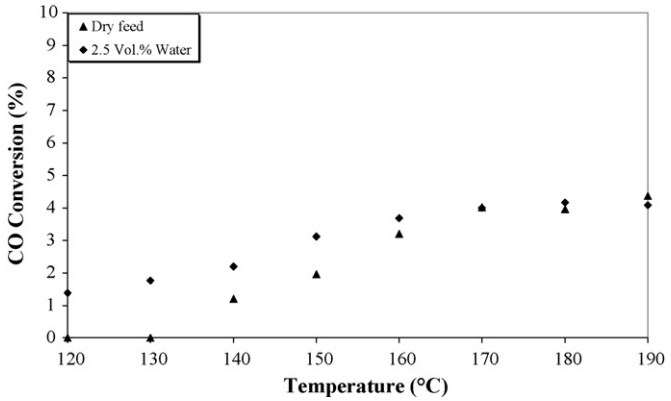

Fig. 9. Effect of steam on CO conversion (0.5 vol.% CO, λ = 2, 60 vol.% H_2, 15 vol.% CO_2 2.5 vol.% H_2O and N_2 in balance).

window from 130 °C to 160 °C the O_2 and H_2 consumption was also negligible. However, the effect is limited to the temperature range between 130 °C and 160 °C.

This is in good agreement with studies of similar catalysts from our group [20]. For the purpose of the present studies, the temperature range between 130 °C and 160 °C was not further investigated and the effect of H_2O not included into the kinetic experiments.

Several authors have proposed an enhancement of the CO oxidation rate in the presence of steam [20,34].

Similar observations have been made by Manasilp and Gulari [35] who investigated CO oxidation over a Pt/Al_2O_3 catalyst and by Yan et al. [36] who investigated CO oxidation over a $Pt–Co/Al_2O_3$ catalyst. Manasilp and Gulari [19,35] proposed the possibility that the OH^- groups formed on the catalyst upon H_2O adsorption are better oxidants than O_2 itself. An interesting mechanism for the influence of OH^- groups on a Pt/SnO_x catalyzed CO oxidation reaction has also been suggested by Schryer et al. [37] where modification of the Pt^0 and $Pt(O)_x$ sites takes place. They proposed that OH^- groups on the surface of a Pt/SnO_2 catalyst (which are regarded as being a significant constituent of tin oxide surfaces) participate in the oxidation of CO chemisorbed on adjacent Pt sites.

Upon increasing the temperature, the rate of CO desorption increases, and thus the number of catalyst sites for O_2 adsorption, is increased. CO oxidation activity therefore, increases [3,38].

4.2.5. Comparison with literature values

The reaction orders determined in this study for CO and O_2 are summarized in Table 11 and compared with the respective values for several other Pt or Rh catalysts.

Generally, α index was always negative, while β in the most cases positive and near 1. Activation energy, E_A, varies from 80 to 130 kJ/mole. The results from [22,23] come closest to the present kinetics. The parameters of these references were determined in presence of a surplus of H_2 similar to the present study.

4.3. Kinetic model development for H_2 oxidation reaction

The H_2 oxidation in the presence of CO (or CO_2) was difficult to be determined because of the phenomena taking place on the surface of the catalyst, mentioned in Section 4.2.2. In the absence of CO, H_2 oxidation over the Pt surface is instantaneous, even at room temperature, and is difficult to control [23]. However, with CO in the feed mixture, CO covers the metal surface and inhibits the H_2 oxidation. The CO_{ad} coverage depends on the temperature. In an adsorption study of CO on a Pt catalyst [23], the full coverage of CO was observed at temperatures below 180 °C [3]. This also

Table 11
Comparison between literature data for CO oxidation rate

Reference	Reaction conditions	T-range (°C)	α	β	γ	E_A (kJ/mole)
[39][e]	Without H_2	<200	−1.5	−1.0		101
[39][e]	0–1 vol.% H_2	<200	−0.7	0.7	−0.2	83
[40][e]	Without H_2	<170	0 to −0.6	1.0		80
[41][e]	Without H_2	>280	−0.6	1.0		125
[42][e]	Without H_2	>230	−0.9	1.0		138
[43][f]	Without H_2	~220	−1.0	1.0		106
[44][c]	Without H_2	>200	−0.8	0.9		103
[44][d]	Without H_2	>180	−0.2	0.9		56
[23][e]	50 vol.% H_2	150–350	−0.5	0.8		78
[22][e]	75 vol.% H_2	150–250	−0.4	0.8		71
This study	Without H_2	150–190	−0.53	0.79		94.2
This study	60 vol.% H_2	150–190	−0.63	0.98	0.0	93.2
This study	60 vol.% H_2 20 vol.% CO_2	160–190	−0.58	0.88	0.0	92.9

Indexes e, f, c and d denote, respectively, $Pt/\gamma\text{-}Al_2O_3$, Rh(1 1 1), Rh/SiO_2, and Pt/SiO_2.

illustrates the limitations in giving values for the activation energy for H_2 oxidation. Despite this inhibition, the reaction rates of H_2 were extremely high.

The Arrhenius plot shown in Fig. 10a and regression analysis provides the activation energy of 12.73 kJ/mole and the pre-exponential factor of 3054 ml g_{cat}^{-1} s^{-1}, respectively. The model

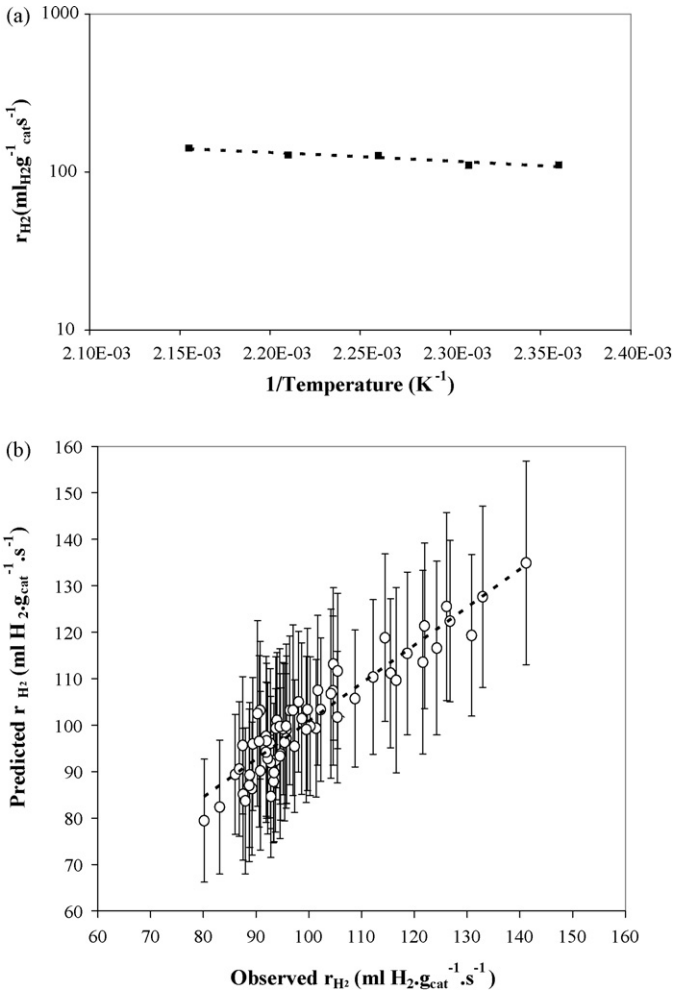

Fig. 10. (a) Arrhenius plot for H_2 oxidation (λ = 4, 1.5 vol.% CO, 40 vol.% H_2 and N_2 in balance) and (b) parity plot for the H_2 oxidation in the presence of CO, O_2, H_2 and N_2 in balance.

Table 12
Models tested for the H_2 oxidation in the presence of CO over Pt–Rh/γ-Al_2O_3 (65 data points)

Model no.	h_1	h_2	h_3	h_4	h_5	h_6	AIC
1.	1	+	+	+	+	+	354.12
2.	+	+	+	–	–	–	312.37
3.	+	–	–	–	–	–	355.46
4.		+	–	–	–	–	372.12
5.	–	–	+	–	–	–	404.83
6.	+	+	–	–	–	–	309.65
7.	+	–	+	–	–	–	424.22
8.	+	–	+	–	+	–	431.54
9.	–	+	+	–	–	–	447.75
10.	–	+	+	+	–	–	428.93
11.	+	+	–	–	–	+	412.91
12.	–	+	–	–	–	+	457.88
13.	+	–	–	–	+	–	303.65
14.	+	–	–	–	–	+	347.27
15.	–	–	–	–	–	–	273.65

Table 13
Confidence intervals of the kinetic parameters of H_2 oxidation in the presence of CO

π	-0.26 ± 0.18
ν	0.09 ± 0.04
κ	-0.06 ± 0.05
E_A (kJ/mole)	12.73 ± 2.84
k_0 ($ml^{1.23}\, g_{cat}^{-1}\, s^{-1}$)	3055 ± 625

proposed to describe the H_2 oxidation in the presence of CO is similar to the model describing CO oxidation:

$$r_{H_2} = \frac{k_0\, e^{-(E_A/RT)}[H_2]^{\pi}[O_2]^{\nu}[CO]^{\kappa}}{(1 + h_1[H_2] + h_2[O_2] + h_3[CO])(1 + h_4[H_2] + h_5[O_2] + h_6[CO])} \quad (25)$$

Similar to the previous cases, the validity of several models was examined which are presented in Table 12.

The model with the lowest AIC score (no. 15) revealed, that the adsorption terms did not improve the quality of the model and were removed consequently. Eq. (25) was modified accordingly.

Following regression analysis of the simplified model we obtained the regression parameters. Confidence interval was 95% and the results are shown in Table 13.

Inserting the values of Table 13 into Eq. (25) we get the final form of the model for the oxidation of H_2:

$$r_{H_2} = 3055\, e^{-(12.73/RT)}[H_2]^{-0.26}[O_2]^{0.09}[CO]^{-0.06}\ ml\, H_2\, g_{cat}^{-1}\, s^{-1} \quad (26)$$

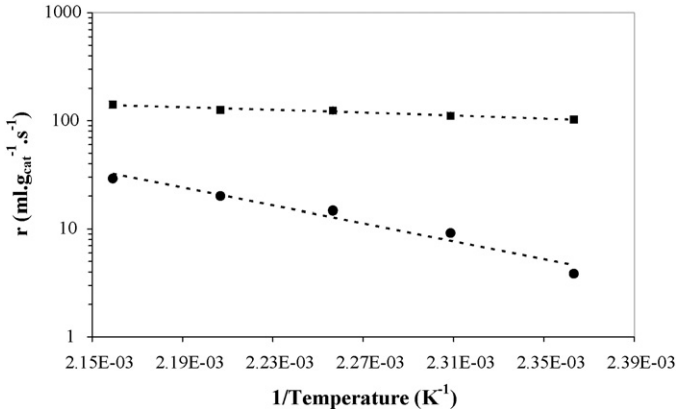

Fig. 11. Arrhenius plot for (●) CO oxidation and (■) H_2 oxidation (λ = 4, 1.5 vol.% CO, 40 vol.% H_2 and N_2 in balance).

The results arising from the model presented by Eq. (26) are in reasonable agreement with data found in literature [45].

The good agreement of the model with the measured data is presented in Fig. 10b. The deviation at higher temperatures of the reaction rate observed from the model was not surprising. At the higher end of temperatures (beyond 170 °C), CO begins to desorb from the catalyst surface resulting in partial coverage of the surface by CO, thus allowing the oxidation of H_2 to proceed at a faster rate [3]. It is also obvious in Fig. 11 that the rate of H_2 oxidation was around 5–10 times higher than that of CO oxidation.

5. Conclusions

To our knowledge, the use of a microreactor operated as recycle reactor for the determination of reaction kinetics is a novel approach. The results compare very well with the same reaction carried out in a fix-bed reactor, as it is reported in literature, which is the common for this kind of studies.

For the estimation of all parameters, a recycle reactor, which has numerous advantages as mentioned in Section 1, was set up. A further benefit persisted in the fact that due to perfect mixing, that can be achieved at high recycle ratios, the material balances were the same as in the ideal, perfectly CSTR. Maintaining the recycle ratio above 25, the reactor behaved like a CSTR, which made the application of simple algebraic equations for the determination of the kinetics possible and thus to simplify the estimation of reaction kinetics.

For the kinetic measurement an "equilibrium" catalyst sample had been used, which had been operated already for 1000 h before. This ensured much higher practical relevance of the kinetic data obtained.

Analysis of the differential data obtained with the catalyst containing 5 wt.% Pt and 5 wt.% Rh over γ-Al_2O_3 resulted in an activation energy ranging from 92.9 kJ/mole to 94.2 kJ/mole, depending on the reaction mixture (within errors these results were adequate). In case where only CO and O_2 are present in the reaction mixture, the exponents α and β, of the partial concentrations, were found to be −0.53 and 0.79, respectively.

By the presence of large amounts of H_2 and CO_2 additional parameters need to be estimated. The reaction rate described by Eq. (24) predicts the preferential oxidation of CO relatively well, independently of the presence or the absence of other reactants such as H_2 and CO_2.

The inhibiting effect of CO_2 and H_2 on both reaction rates (CO and H_2 oxidation), may be explained by the formation of carboxylate, carbonate and hydro-carbonyl species, respectively. The latter species can decrease the reaction rate for both reactions by decreasing the alumina surface available for O_2 adsorption and thus decreasing the concentration of adsorbed O_2 on Rh/alumina. Additionally, high CO_2 and H_2 concentrations, relative to O_2, in reformate may result in a reduced surface coverage. However, at temperatures exceeding the range under investigation in the current paper, an effect of steam partial pressure is to be expected owing to the reverse water-gas shift reaction.

Furthermore, the undesired parallel reaction of the H_2 oxidation was also investigated. Activation energy was found to be approximately 12.7 kJ/mole and the exponents of H_2, O_2 and CO partial concentrations −0.29, 0.09 and −0.06, respectively.

The negative influence of H_2 on both reactions is explained also as an effective removal of active O_2 through water formation. On the other hand, steam has no effect on the catalyst performance at temperatures exceeding 160 °C, whereas it enhances oxidation rates at lower temperatures.

Acknowledgment

The support of part of this work by Deutsche Bundesstiftung Umwelt is gratefully acknowledged.

References

[1] V. Hessel, H. Löwe, A. Müller, G. Kolb, Chemical Micro Process Engineering—Processing and Plants, Wiley–VCH, Weinheim, 2005.
[2] G. Kolb, V. Hessel, V. Cominos, H. Löwe, G. Nikolaidis, R. Zapf, A. Ziogas, E.R. Delsman, M.H.J.M. de Croon, J.C. Schouten, O. de la Iglesia, R. Mallada, J. Santamaria, Catal. Today 120 (2007) 2–20.
[3] S. Srinivas, A. Dhingra, H. Im, E. Gulari, Appl. Catal. A: General 274 (2004) 285–293.
[4] K. Schubert, W. Bier, G. Linder, D. Seider, Chem. Ing. Tech. 61 (1989) 172–173.
[5] G. Ondrey, Chem. Eng. J. 56 (2001) 293–303.
[6] K. Jähnisch, V. Hessel, H. Löwe, M. Baerns, Angew. Chem. Int. Ed. 43 (2004) 406–446.
[7] G. Kolb, R. Zapf, V. Hessel, H. Löwe, Appl. Catal. A 277 (2004) 155–166.
[8] W. Ehrfeld, V. Hessel, H. Löwe, Microreactors: New Technology for Modern Chemistry, Wiley–VCH, Weinheim, Germany, 2000.
[9] L. Kiwi-Minsker, A. Renken, Catal. Today 110 (2005) 2–14.
[10] K. Shah, X. Ouyang, R.S. Besser, Chem. Eng. and Technol. 28 (2005) 303–313.
[11] E.G. Christoffel, Catal. Rev.-Sci. Eng. 24 (1982) 159–232.
[12] L.K. Doraiswamy, Catal. Rev.-Sci. Eng. 10 (1974) 177–219.
[13] J.M. Berty, Catal. Rev.-Sci. Eng. 20 (1979) 75–96.
[14] O. Levenspiel, Chemical Reaction Engineering, Third edition, John Wiley & Sons, 1999.
[15] M. Čurlin, H. Korajlija, M. Matošić, I. Mijatović, Ž. Kurtanjek, Effect of hydraulic residence time and mixing on wastewater treatment in a membrane bioreactor, 1st EMCO Workshop, Dubrovnik, Croatia, October 20–21, 2005.
[16] S.H. Oh, G.B. Fisher, J.E. Carpenter, D.W. Goodman, J. Catal. 100 (1996) 360–376.
[17] School of Biological and Chemical Sciences, Queen Mary, University of London, Mile End Road, London E1 4NS. Stand July 2007, http://www.chem.qmul.ac.uk/surfaces/scc/.
[18] R.H. Nibbelke, M.A. Campman, J.H.B.J. Hoebink, G.B. Marin, J. Catal. 171 (1997) 358–373.
[19] Hurvey Motulsky, Arthur Christopoulos, Fitting models to biological data using linear and nonlinear regression, Oxford University Press, 2004.
[20] V. Cominos, V. Hessel, C. Hofmann, G. Kolb, R. Zapf, A. Ziogas, E.R. Delsman, J.C. Schouten, Catal. Today 110 (2005) 140–153.
[21] R. Zapf, C. Becker-Willinger, K. Berresheim, H. Bolz, H. Gnaser, V. Hessel, G. Kolb, P. Löb, A.-K. Pannwitt, A. Ziogas, I. Chem. Eng. 81 (2003) 721–729.
[22] M.J. Kahlich, H.A. Gasteiger, R.J. Behm, J. Catal. 171 (1997) 93–105.
[23] D.H. Kim, M.S. Lim, Appl. Catal. A: General 224 (2002) 27–38.
[24] K. Grass, H.-G. Lintz, J. Catal. 172 (1997) 446–452.
[25] K.H. Yang, O.A. Hougen, Chem. Eng. Prog. 46 (1950) 146–157.
[26] L. Irving, T. Faraday Soc. 17 (1922) 621–654.
[27] B. Riedmüller, D.C. Papageorgopoulos, B. Berenbak, R.A. van Santen, A.W. Kleyn, Surf. Sci. 515 (2002) 323–336.
[28] X. Liu, O. Korotkith, R. Farrauto, Appl. Catal. A: General 226 (2002) 293–303.
[29] T. Ioannides, X. Verykios, J. Catal. 140 (1993) 353–369.
[30] J.T. Yates, P.A. Thiel, W.H. Weinberg, Surf. Sci. 82 (1979) 45–68.
[31] G. Avgouropoulos, T. Ioannides, H.K. Matralis, J. Batista, S. Hocevar, Catal. Lett. 73 (2001) 33–40.
[32] G. Avgouropoulos, T. Ioannides, Appl. Catal. A: General 244 (2003) 155–167.
[33] T. Ince, G. Uysal, A.N. Akin, R. Yildirim, Appl. Catal. A: General 292 (2005) 171–176.
[34] R.J.H. Grisel, B.E. Nieuwenhuys, J. Catal. 199 (2001) 48–59.
[35] A. Manasilp, E. Gulari, Appl. Catal. B: Environ. 37 (2002) 17–25.
[36] J. Yan, J. Ma, P. Cao, P. Li, Catal. Lett. 93 (2004) 55.
[37] D.R. Schryer, B.T. Upchurch, B.D. Sidney, K.G. Brown, G.B. Hoflund, R.K. Herz, J. Catal. 130 (1991) 314.
[38] C.D. Dudfield, R. Chen, P.L. Adcock, J. Power Sources 85 (2000) 237–244.
[39] H. Muraki, S. Matunaga, H. Shinjoh, M. Wainwright, J. Chem. Technol. Biotechnol. 52 (1991) 415–424.
[40] P.J. Berlowitz, C.H.F. Peden, D.W. Goodman, J. Phys. Chem. 92 (1988) 5213–5221.
[41] G.S. Zafiris, R.J. Gorte, J. Catal. 140 (1993) 418–423.
[42] J.A. Rodriguez, D.W. Goodmann, Surf. Sci. Rep. 14 (1991) 1–107.
[43] C.H.F. Peden, D.W. Goodman, D.S. Blair, P.J. Berlowitz, G.B. Fisher, S.H. Oh, J. Phys. Chem. 92 (1988) 1563–1567.
[44] N.W. Cant, P.C. Hicks, B.S. Lennon, J. Catal. 54 (1978) 372–383.
[45] V.V. Gorodetskii, G.I. Panov, V.A. Sobyanin, N.N. Bulgakov, React. Kinet. Catal. Lett. 9 (1978) 239–244.